Photochemical Activation of CO_2 on $Rh^I(CO)_2/Al_2O_3$−CO_2 Dissociation and Oxygen Atom Exchange

Edward A. Wovchko and John T. Yates, Jr.

Contribution from the Surface Science Center, Department of Chemistry, University of Pittsburgh, Pittsburgh, Pennsylvania 15260

Received February 5, 1998

Abstract: The ultraviolet (3.8 eV) photolysis of atomically dispersed $Rh^I(^{13}C^{18}O)_2$ species supported on an Al_2O_3 surface in the presence of CO_2 at 256 K has been studied by infrared spectroscopy (FTIR). Carbon dioxide is activated on photochemically produced $Rh^I(^{13}C^{18}O)$ sites to produce various isotopically labeled rhodium *gem*-dicarbonyl species. The two major products of CO_2 activation exhibit infrared bands at 2077 and 1958 cm^{-1} assigned to $Rh^I(^{12}C^{16}O)(^{13}C^{18}O)$ species and bands at 2036 cm^{-1} and near 1958 cm^{-1} assigned to $Rh^I(^{13}C^{16}O)(^{13}C^{18}O)$. The infrared band assignments for the isotopic rhodium *gem*-dicarbonyl species are supported by a thermally driven isotopic exchange experiment with $^{13}C^{16}O(g)$ and by a comparison to the frequencies predicted with frequency calculations based on known force constants. Two dissociation pathways are proposed for CO_2 coordinated on $Rh^I(^{13}C^{18}O)$ sites. Path I involves direct dissociation of the C−O bond in CO_2 and Path II involves oxygen atom exchange between CO_2 and CO ligands, followed by C−O bond dissociation in the CO_2 ligand which was produced by the O exchange process. The lack of formation of oxidized rhodium carbonyl species during CO_2 activation suggests that CO_2 temporarily coordinates to $Rh^I(CO)$ with η^1 bonding. This work demonstrates the first steps of a potential low-temperature route for the conversion of CO_2 into other molecules on catalyst sites using ultraviolet light as an energy source.

1. Introduction

The thermodynamic stability of CO_2 contributes to the general lack of commercial processes that utilize CO_2 as a feedstock. One method of overcoming the stability is to utilize ultraviolet light as an alternative source of energy to conventional thermal energy sources. The photochemical production of surface sites, capable of activating bonds such as the C−H bond in alkanes, and the C−O bond in CO_2 provides an interesting and potentially useful route to the utilization of methane and CO_2 as feedstocks to other useful products. We have carried out experiments to study heterogeneous phase bond activation using the species $Rh^I(CO)_2$, on Al_2O_3 supports (designated $Rh^I(CO)_2/Al_2O_3$). By photolyzing the $Rh^I(CO)_2$ species with 325 nm (3.8 eV) ultraviolet light at low temperatures (<300 K), a CO ligand is easily detached to produce a monocarbonyl species, $Rh^I(CO)$. This proposed 16-electron coordinatively unsaturated Rh^I center adsorbs dinitrogen,[1] and breaks the C−H bond in alkanes[2−5] and the H−H bond in hydrogen.[6] In this study, we have successfully activated the C−O bond of carbon dioxide using the photochemical production of $Rh^I(CO)$ sites.

Several recent reviews discuss the chemistry of CO_2 on metal and metal oxide surfaces[7,8] as well as the coordination and chemistry of CO_2 with transition metal complexes.[9−11] Dissociation of CO_2 occurs on several metal surfaces, including Fe, Ni, Re, Al, and Mg, but to little or no extent on Pt and *pure* Rh.[7,8] In the presence of alkali metals such as potassium, CO_2 dissociation on Rh occurs readily.[12] Photoexcitation of alkali-promoted Rh surfaces also causes adsorbed CO_2 dissociation through substrate-mediated excitation; however, no dissociation was observed on a clean Rh surface.[13] It is suggested that dissociation occurs via electron transfer from the alkali metal/Rh surface to create $CO_2^{\delta-}$ anions with a bent geometry.[7,8,13] The surface-coordinated CO_2 molecule is then subject to activation and subsequent reaction with other adsorbates. There are numerous examples of organometallic compounds that involve transition metals containing CO_2 ligands.[9−11] However, only a few fully characterized examples of CO_2 directly coordinated to a single Rh center are reported.[9−11,14−16] The best example of a rhodium η^1-CO_2 complex is $Rh(diars)_2(Cl)(CO_2)$ [diars = *o*-phenylene-bis(dimethylarsine)] reported by Herskovitz and co-workers.[14] There have been few reports of the photochemistry of transition metal−carbon dioxide complexes.[9] One study, involving the photolysis of $Cp_2Mo(CO_2)$ in the presence of CO_2, resulted in the formation of $Cp_2Mo(CO_3)$, $Cp_2Mo(CO)$ and CO.[17]

There have been several studies of the CO_2 adsorption on supported Rh catalysts.[18−20] No dissociation of CO_2 was

(1) Wovchko, E. A.; Yates, J. T., Jr. *J. Am. Chem. Soc.* **1996**, *118*, 10250.
(2) Ballinger, T. H.; Yates, J. T., Jr. *J. Am. Chem. Soc.* **1992**, *114*, 10074.
(3) Ballinger, T. H.; Yates, J. T., Jr. *J. Phys. Chem.* **1992**, *96*, 9979.
(4) Wong, J. C. S.; Yates, J. T., Jr. *J. Am. Chem. Soc.* **1994**, *116*, 1610.
(5) Wong, J. C. S.; Yates, J. T., Jr. *J. Phys. Chem.* **1995**, *99*, 12640.
(6) Wovchko, E. A.; Yates, J. T., Jr. *J. Am. Chem. Soc.* **1995**, *117*, 12557.
(7) Freund, H.-J.; Roberts, M. W. *Surf. Sci. Rep.* **1996**, *25*, 225.
(8) Solymosi, F. *J. Mol. Catal.* **1991**, *65*, 337.
(9) Gibson, D. H. *Chem. Rev.* **1996**, *96*, 2063.
(10) Leitner, W. *Coord. Chem. Rev.* **1996**, *153*, 257.
(11) Behr, A. *Carbon Dioxide Activation by Metal Complexes*; VCH Verlagsgesellschaft mbH: Weinheim, Germany, 1988.
(12) Kiss, J.; Révész, K.; Solymosi, F. *Surf. Sci.* **1988**, *207*, 36.
(13) Solymosi, F.; Klivényi, G. *J. Phys. Chem.* **1994**, *98*, 8061.
(14) Calabrese, J. C.; Herskovitz, T.; Kinney, J. B. *J. Am. Chem. Soc.* **1983**, *105*, 5914.
(15) Vigalok, A.; Ben-David, Y.; Milstein, D. *Organometallics* **1996**, *15*, 1839.
(16) Aresta, M.; Nobile, C. F. *Inorg. Chim. Acta* **1977**, *24*, L49.
(17) Belmore, K. A.; Vanderpool, R. A.; Tsai, J.-C.; Khan, M. A.; Nicholas, K. M. *J. Am. Chem. Soc.* **1988**, *110*, 2004.
(18) Solymosi, F.; Erdöhelyi, A.; Kocsis, M. *J. Catal.* **1980**, *65*, 428.
(19) Henderson, M. A.; Worley, S. D. *Surf. Sci.* **1985**, *149*, L1.

S0002-7863(98)00411-9 CCC: $15.00
Published on Web 07/17/1998

observed on clean samples at 300 K. Hydrogenation of CO_2 into methane occurs at elevated temperature (>300 K) and to a greater extent at temperatures near 500 K.[18,20,21] Various rhodium carbonyl species were detected as a result of CO_2 dissociation during a reaction with hydrogen. A considerable amount of research has been conducted on the reforming of methane with CO_2 into synthesis gas (H_2 + CO).[22−26] The conversion takes place on a variety of catalysts including supported rhodium, but temperatures around 1000 K are necessary. The above studies demonstrate the need for an alternative method to activate CO_2 on supported catalysts.

In this paper, we have employed infrared spectroscopy and ultrahigh vacuum techniques to investigate the ultraviolet photolysis of $Rh^I(^{13}C^{18}O)_2/Al_2O_3$ in the presence of carbon dioxide at 256 K. Carbon dioxide dissociation occurs on the atomically dispersed photochemically generated $Rh^I(^{13}C^{18}O)$ species leading ultimately to the production of $Rh^I(^{12}C^{16}O)$-$(^{13}C^{18}O)$ and, through oxygen-atom exchange, $Rh^I(^{13}C^{16}O)$-$(^{13}C^{18}O)$ species. The latter species are identified by comparing infrared spectra measured during photolysis to those measured during a thermal exchange of isotopically labeled $^{13}C^{16}O$ gas with $Rh^I(^{13}C^{18}O)_2$. Assignments of the various isotopomers of $Rh^I(CO)_2$ are supported by comparing infrared band frequencies to the predicted normal-mode frequencies of $Rh^I(CO)_2$ (C_{2v}) by using force constant calculations. The CO_2 activation was also compared to the photochemically assisted oxidation by O_2 of $Rh^I(^{13}C^{18}O)_2/Al_2O_3$. A mechanism for CO_2 activation on Rh^I-(CO) sites is proposed.

2. Experimental Section

Experiments were conducted in the special transmission infrared cell described in detail previously.[27,28] The cell is a stainless steel cube with six conflat flange ports. KBr windows, sealed with differentially pumped double O-rings, were used on two ports for infrared beam transmission. A UV-grade quartz window was used for ultraviolet irradiation. Samples were spray deposited on a tungsten support grid (0.0254 mm thick with 0.22 mm square openings exhibiting 70% optical transparency). The grid was secured by nickel clamps and mounted on electrical feedthroughs mounted on the bottom of a reentrant Dewar that enters the cell. The sample was heated electrically with a digital temperature programmer/controller.[29] For CO_2 activation experiments, sample cooling was achieved by filling the reentrant Dewar with an ethanol slush cooled by inserting a tube conducting a mixture of flowing N_2 liquid and gas. For O_2 activation in separate experiments, the Dewar was filled with liquid nitrogen. Sample temperatures were measured by a K-type thermocouple spot welded on the top center of the tungsten grid. The temperature could be held constant and maintained to ±2 K in the range 150 to 1500 K. The cell was connected via stainless steel bellows tubing to a bakeable stainless steel vacuum and gas delivery system. The system was pumped by 60 L s^{-1} turbomolecular and 30 L s^{-1} ion pumps, achieving base pressures $<1 \times 10^{-8}$ Torr. The system was equipped with a Dycor M100M quadrupole mass spectrometer for gas analysis and leak checking. Gas pressures were measured with a MKS 116A Baratron capacitance manometer.

The 0.5% Rh/Al_2O_3 samples were prepared by dissolving $RhCl_3 \cdot 3H_2O$ (Alfa 99.9%) in ultrapure H_2O (10 mL/g of support). The solution was mixed with the appropriate amount of powdered Al_2O_3 (Degussa, 101 m^2/g) and ultrasonically dispersed for approximately 45 min. This slurry was mixed with acetone (Mallinckrodt, AR) (9/1 acetone/H_2O volume ratio) and sprayed onto the tungsten grid with a nitrogen-gas pressured atomizer. The grid was warm (~330 K) and spraying was interrupted intermittently to allow for solvent evaporation. The mixture was sprayed on a 2/3 section (3.0 cm^2) of the grid leaving a shielded 1/3 (1.5 cm^2) section clear for background scans. Deposit weights ranged from 28.5 to 29.1 mg (9.5 to 9.7 mg/cm^2) depending on the spraying time.

Immediately after spraying, the sample was transferred to the infrared cell and evacuated at 475 K for 16−20 h. Following evacuation the sample was reduced at 475 K with three 175 Torr H_2 exposures of 15 min each, and one 200 Torr H_2 exposure of 60 min duration with evacuation after each exposure. The sample was evacuated at 475 K for another 18 to 20 h then cooled to 303 K and exposed to 5 Torr of $^{13}C^{18}O$ for 10 min to convert the metallic Rh to $Rh^I(^{13}C^{18}O)_2$. The cell was evacuated and the sample was cooled to 238 K prior to carbon dioxide addition (and 110 K prior to O_2 addition). After addition, the sample was warmed to 256 K (181 K for the O_2 experiment). The temperature never exceeded 258 K during each experiment.

Infrared spectra were measured by using a nitrogen-gas purged Mattson Research Series I Fourier transform infrared spectrometer equipped with a liquid nitrogen cooled HgCdTe wide band detector. Spectra were recorded by averaging 250 scans at 4 cm^{-1} spectral resolution, respectively. The cell was translated laterally so the beam could pass through the unsprayed portion of the grid to obtain the background spectra. Small background features due to small deposits on the KBr windows were observed. Absorbance spectra of the sample were obtained by ratioing single beam spectra of the sample to background single beam spectra. All spectra were baseline corrected.

A 350 W high-pressure mercury arc lamp provided the ultraviolet light for photolysis experiments. The optical bench was equipped with a *f*/1 two-element UV fused silica condensing lens, an iris diaphragm, and a shutter. The light was filtered by a 10 cm water infrared radiation filter and a 3.8 ± 0.5 eV (325 ± 50 nm) band-pass filter. Thermopile measurements indicate that the photofluxes of the filtered UV light were 7.4×10^{16} photons cm^{-2} s^{-1} ± 10%. Photochemistry and infrared measurements were conducted simultaneously without disturbing the position of the cell or UV lamp. This was done by orienting the UV light source perpendicular to the infrared beam. The tungsten grid was aligned such that the infrared beam and the UV light were focused at a 45° angle to the normal of the grid.[28]

Isotopically labeled $^{13}C^{18}O$ (Icon, 99% ^{13}C, 95% ^{18}O) and $^{13}C^{16}O$ (Cambridge, 99.5% ^{13}C) were obtained in glass breakseal flasks and were used without further purification. Carbon dioxide (Matheson, 99.995%) and oxygen (Matheson, 99.998%) were obtained in steel cylinders and transferred to previously evacuated and baked glass bulbs and used without further purification. Hydrogen (Matheson, 99.9995%) was obtained in a steel cylinder and was also used without further purification.

3. Results

1. Photolysis of $Rh^I(^{13}C^{18}O)_2/Al_2O_3$ in CO_2. Infrared spectra corresponding to the photolysis of $Rh^I(^{13}C^{18}O)_2$ supported on Al_2O_3 in the presence of CO_2 at an equilibrium pressure of 1 Torr and a sample temperature of 256 K are shown in Figure 1. The initial spectrum measured prior to any UV light exposure ($t_{UV} = 0$ min) shows two infrared bands at 2003 and 1936 cm^{-1} in the C−O region for the respective symmetric and antisymmetric stretching modes of isotopically labeled Rh^I-$(^{13}C^{18}O)_2$ (rhodium gem-dicarbonyl).[1] The formation of isolated $Rh^I(^{13}C^{18}O)_2$ occurs from the disruption of metallic Rh in a reaction with isotopically labeled $^{13}C^{18}O$ and hydroxyl groups

(20) Solymosi, F.; Pásztor, M. *J. Catal*. **1987**, *104*, 312.
(21) Henderson, M. A.; Worley, S. D. *J. Phys. Chem*. **1985**, *89*, 1417.
(22) Edwards, J. H.; Maitra, A. M. *Fuel Processing Technol.* **1995**, *42*, 269.
(23) Wang, S.; Lu, G. Q. (Max); Millar, G. J. *Energy Fuels* **1996**, *10*, 896.
(24) Muir, J. F.; Hogan, R. E., Jr.; Skocypec, R. D.; Buck, R. *Solar Energy* **1994**, *52*, 467.
(25) Erdöhelyi, A.; Cserényi, J.; Solymosi, F. *J. Catal*. **1993**, *141*, 287.
(26) Bhat, R. N.; Sachtler, W. M. H. *Appl. Catal. A: Gen*. **1997**, *150*, 279.
(27) Basu, P.; Ballinger, T. H.; Yates, J. T., Jr. *Rev. Sci. Instrum*. **1988**, *59*, 1321.
(28) Wong, J. C. S.; Linsebigler, A.; Lu, G.; Fan, J.; Yates, J. T., Jr. *J. Phys. Chem*. **1995**, *99*, 335.
(29) Muha, R. J.; Gates, S. M.; Yates, J. T., Jr.; Basu, P. *Rev. Sci. Instrum.* **1985**, *56*, 613.

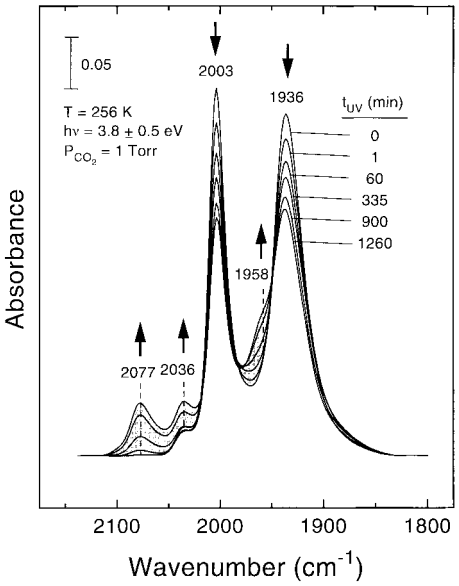

Figure 1. Infrared spectra measured in the C−O stretching region during 1260 min of photolysis of $Rh^I(^{13}C^{18}O)_2/Al_2O_3$ in the presence of 1 Torr of CO_2 at 256 K. The arrows indicate the direction of the absorbance changes and shaded regions indicate new features.

(Al−OH) on the Al_2O_3 support.[30,31] The infrared bands at 2003 and 1936 cm^{-1} are appropriately shifted to lower frequencies compared to the unlabeled $Rh^I(CO)_2$ species with infrared bands at 2099 and 2028 cm^{-1}.[32−38] (Note that the CO and CO_2 designation corresponds to $^{12}C^{16}O$ and $^{12}C^{16}O_2$ in natural abundance.) A small band is observed at 2036 cm^{-1} for $Rh^I(^{13}C^{16}O)(^{13}C^{18}O)$ species due to the 5% $^{13}C^{16}O$ impurity in the isotopically labeled $^{13}C^{18}O$. A single infrared band centered at 2344 cm^{-1} (not shown) is indicative of CO_2 adsorbed onto the Al_2O_3 support.[39,40] (The intensity of this band, indicating the extent of CO_2 adsorption, varies with subtle changes in the temperature and did not necessarily reflect changes that occurred in the C−O stretching region.)

The UV lamp shutter was opened, allowing the sample to be irradiated, and infrared spectra were measured at the indicated times (t_{UV}) during 1260 min of ultraviolet photolysis. The absorbance of the two bands at 2003 and 1936 cm^{-1} continually decreases (the direction is shown by the heavy arrows), indicating the depletion $Rh^I(^{13}C^{18}O)_2$ species. The depletion is accompanied by the development of two overlapping infrared bands centered at 2077 and 2036 cm^{-1} (shaded for better visualization). These bands lie within the C−O stretching region for various isotopic mixtures of rhodium carbonyl species.[36,41] An infrared band growing at 1958 cm^{-1} (also shaded) overlaps the band at 1936 cm^{-1} for $Rh^I(^{13}C^{18}O)_2$ species that is decreasing in intensity during irradiation. The formation of these bands is indicative of the activation of the C−O bond in CO_2 to produce rhodium gem-dicarbonyl species with various CO isotopomers.

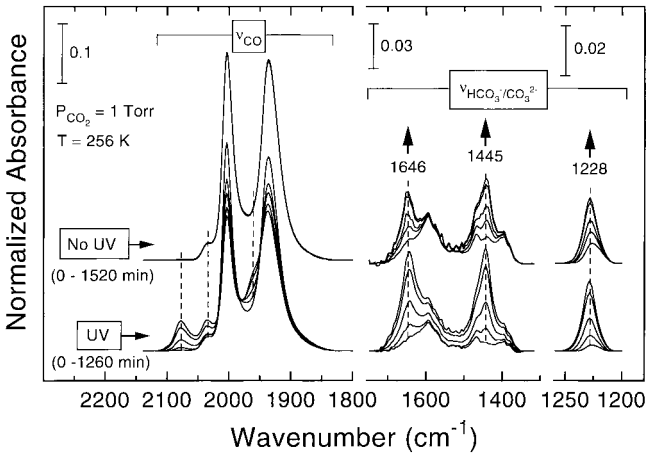

Figure 2. Comparison of carbonyl and bicarbonate/carbonate infrared stretching frequencies during photochemical activation and thermal adsorption of CO_2 on $Rh^I(^{13}C^{18}O)_2/Al_2O_3$ at 256 K. The upper set of infrared spectra were measured during 1520 min of CO_2 exposure *in the absence* of ultraviolet light. The lower set of spectra (spectra from Figure 1) were measured during 1260 min *with* UV irradiation.

To distinguish photochemical events from thermal events, the spectra measured during ultraviolet irradiation in Figure 1 are compared in Figure 2 to normalized infrared spectra measured during 1520 min of CO_2 exposure to $Rh^I(^{13}C^{18}O)_2/Al_2O_3$ at 256 K *without* exposure to ultraviolet light (upper set of spectra normalized to the absorbance at 2003 cm^{-1} of the initial spectrum prior to photolysis). One observes that essentially no changes take place in the carbonyl stretching region for the infrared spectra recorded in the absence of ultraviolet light. However, bands develop at 1646, 1445, and 1228 cm^{-1} in both experiments. Bands in this region may be assigned to bicarbonate and carbonate species adsorbed on the Al_2O_3 support. Depending on the type of alumina and the degree of hydroxylation, the 1646 cm^{-1} band, 1228 cm^{-1} band, and features around 1470 cm^{-1} are generally assigned to bicarbonate species produced in a reaction of CO_2 with hydroxyl groups.[39,40,42] The feature at 1445 cm^{-1} is assigned to "free" carbonates presumably produced in a reaction of CO_2 with surface oxide ions.[39,42] Qualitatively similar spectral developments take place in the HCO_3/CO_3 region in both the irradiated and nonirradiated cases. No isotopically substituted bicarbonate or carbonate species are observed, indicating that the adsorption of CO_2 to form bicarbonates/carbonates is predominantly a support process occurring on the Al_2O_3 and is not dependent on the photochemically induced activation of CO_2 on Rh sites.

2. Isotopic Thermal Exchange: $Rh^I(^{13}C^{18}O)_2 + {}^{13}C^{16}O$. Infrared spectra measured during the thermal exchange of $^{13}C^{16}O$ with $Rh^I(^{13}C^{18}O)_2/Al_2O_3$ are presented in Figure 3. The spectra shift systematically to higher frequency as the number of $^{13}C^{16}O$ molecules added is increased from 6×10^{18} molecules to 5×10^{19} molecules and the temperature is raised from 222 to 300 K. Similar to the isotopic exchange process with $Rh^I(CO)_2$ and $^{12}C^{18}O$ reported by Yates and Kolasinski,[36] six infrared bands are observed as the exchange takes place, representing three isotopic rhodium gem-dicarbonyl species: $Rh^I(^{13}C^{18}O)_2$, $Rh^I(^{13}C^{16}O)(^{13}C^{18}O)$, and $Rh^I(^{13}C^{16}O)_2$. Each species is responsible

(30) Basu, P.; Panayotov, D.; Yates, J. T., Jr. *J. Phys. Chem.* **1987**, *91*, 3133.
(31) Basu, P.; Panayotov, D.; Yates, J. T., Jr. *J. Am. Chem. Soc.* **1988**, *110*, 2074.
(32) Yang, A. C.; Garland, C. W. *J. Phys. Chem.* **1957**, *61*, 1504.
(33) Yates, J. T., Jr.; Duncan, T. M.; Worley, S. D.; Vaughan, R. W. *J. Chem. Phys.* **1979**, *70*, 1219.
(34) Yates, J. T., Jr.; Duncan, T. M.; Vaughan, R. W. *J. Chem. Phys.* **1979**, *71*, 3908.
(35) Cavanagh, R. R.; Yates, J. T., Jr. *J. Chem. Phys.* **1981**, *74*, 4150.
(36) Yates, J. T., Jr.; Kolasinski, K. *J. Chem. Phys.* **1983**, *79*, 1026.
(37) Rice, C. A.; Worley, S. D.; Curtis, C. W.; Guin, J. A.; Tarrer, A. R. *J. Chem. Phys.* **1981**, *74*, 6487.
(38) Solymosi, F.; Pásztor, M. *J. Phys. Chem.* **1985**, *89*, 4789.
(39) Parkyns, N. D. *J. Phys. Chem.* **1971**, *75*, 526.
(40) Peri, J. B. *J. Phys. Chem.* **1966**, *70*, 3168.
(41) Knözinger, H.; Thornton, E. W.; Wolf, M. *J. Chem. Soc., Faraday Trans. 1* **1979**, *75*, 1888.
(42) Schubart, W.; Knözinger, H. *Z. Phys. Chem. Neue Folge* **1985**, *144*, 117.

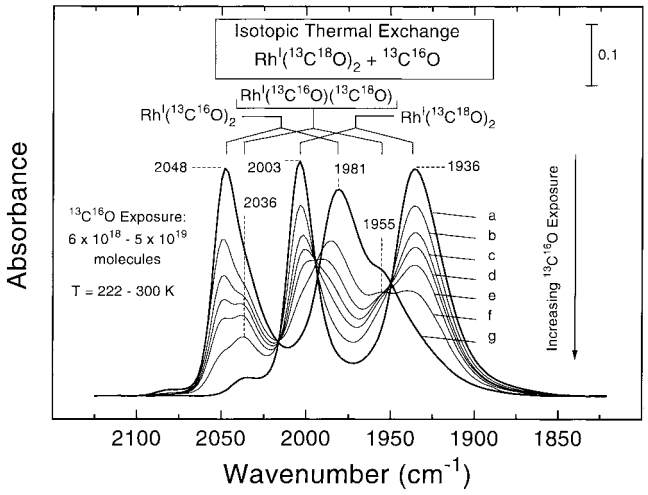

Figure 3. Isotopic thermal exchange reaction between $^{13}C^{16}O$ gas and $Rh^I(^{13}C^{18}O)_2/Al_2O_3$. Infrared spectra were recorded over a temperature range of 222−300 K while simultaneously increasing the number of $^{13}C^{16}O$ molecules added to the cell from 6×10^{18} molecules to 5×10^{19} molecules. The order of spectral recording (a−g) and direction of increasing $^{13}C^{16}O$ coverage are indicated by the arrow.

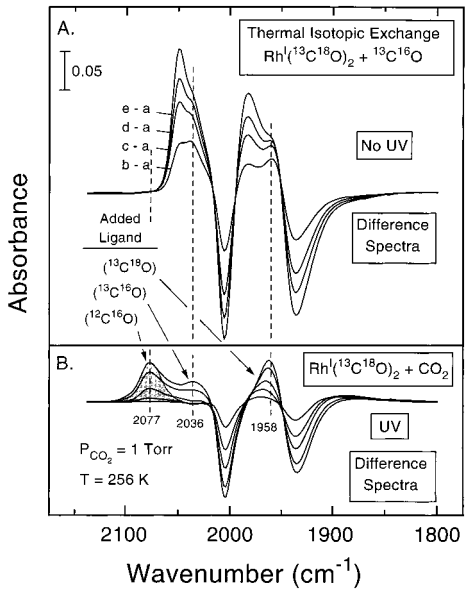

Figure 4. Comparison of $^{13}C^{16}O$ thermal isotopic exchange to photoassisted CO_2 activation. Part A: Selected difference spectra from Figure 3 measured during initial stages of $^{13}C^{16}O$ exposure. Part B: Difference spectra from Figure 1 measured during photolysis of CO_2 and $Rh^I(^{13}C^{18}O)_2$.

for two of the six infrared bands. The assignments and frequencies are indicated in Figure 3. Note that errors are inherent in the measurement of the frequencies for the mixed isotopic species, $Rh^I(^{13}C^{16}O)(^{13}C^{18}O)$, since the two infrared bands of this species are always overlapped by the neighboring features.

A more definitive picture of the sequential developments during thermal isotopic exchange is obtained by examining the difference spectra for the first stages of isotopic exchange shown in part A of Figure 4. The initial spectrum measured prior to $^{13}C^{16}O$ exposure (spectrum a) has been subtracted from the subsequent spectra. The negative development of spectral features indicate the depletion of $Rh^I(^{13}C^{18}O)_2$ and positive developments indicate the isotopic exchange and increase in $^{13}C^{16}O$ content. Note that the frequencies of the developing bands do not shift as their absorbance increases.

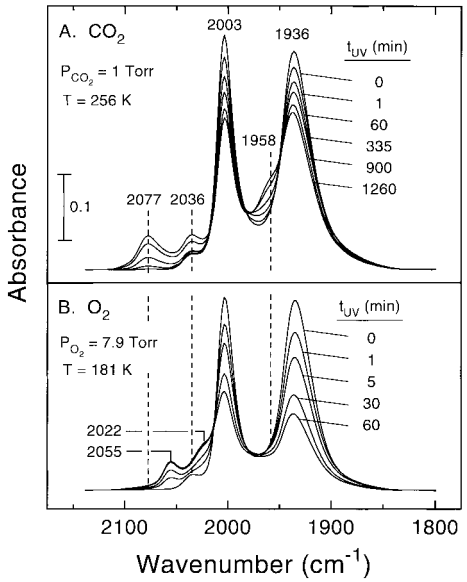

Figure 5. Comparison of CO_2 activation to photoassisted oxidation of $Rh^I(^{13}C^{18}O)_2/Al_2O_3$. Part A: Infrared spectra from Figure 1 measured during 1260 min of photolysis at 256 K. Part B: Infrared spectra recorded during 60 min of photolysis in the presence of 7.9 Torr of O_2 at 181 K.

Figure 4B shows difference spectra measured from Figure 1 during ultraviolet irradiation of $Rh^I(^{13}C^{18}O)_2/Al_2O_3$ in the presence of CO_2. Here also the initial spectrum ($t_{UV} = 0$ min) has been subtracted from the subsequent spectra. Once again the formation of positive infrared features occurs at 2077, 2036, and 1958 cm^{-1}. The negative features represent the depletion of $Rh^I(^{13}C^{18}O)_2$ species. Note that the position of the 1958 cm^{-1} feature shifts to lower frequency as the photolysis progresses. The dashed vertical lines are drawn to show the correlation with features developing during the thermal isotopic exchange in Figure 4A. The 2036 cm^{-1} band measured during photolysis corresponds to the same frequency measured from the unsubtracted spectra of Figure 3 during isotopic exchange. The 1958 cm^{-1} band is also in good agreement with the infrared band at 1955 cm^{-1} of Figures 3 and 4A. The correlation shown in Figures 4A and 4B between these two experiments indicates that $Rh^I(^{13}C^{16}O)(^{13}C^{18}O)$ species are produced during ultraviolet irradiation of $Rh^I(^{13}C^{18}O)_2/Al_2O_3$ in the presence of CO_2(g). The 2077 cm^{-1} feature does not correlate with any infrared bands in the thermal isotopic exchange with $^{13}C^{16}O$ and is due to the activation of CO_2 to produce a $^{12}C^{16}O$-containing surface carbonyl species. This is indicative of an additional photochemical process in which $^{12}C^{16}O_2$ is converted to a $^{12}C^{16}O$ ligand on Rh^I centers.

3. Comparison of CO_2 Photolysis to the Photoassisted Oxidation of $Rh^I(^{13}C^{18}O)_2/Al_2O_3$. In an effort to support the assignment of the 2077 cm^{-1} feature to a $^{12}C^{16}O$-containing species during ultraviolet irradiation of CO_2 rather than to $^{13}C^{16}O$-containing species, the photoassisted oxidation of $Rh^I(^{13}C^{18}O)_2/Al_2O_3$ was conducted with $^{16}O_2$(g) as shown in Figure 5. Part A of Figure 5 displays the infrared spectra measured during CO_2 photolysis in Figure 1. The photoreaction of $Rh^I(^{13}C^{18}O)_2/Al_2O_3$ in the presence of 7.9 Torr of O_2 at 181 K is presented in Figure 5B. One observes two new infrared bands growing at 2055 and 2022 cm^{-1} during 60 min of photolysis in oxygen which do not correspond to the features developing during CO_2 activation, as shown by the dashed lines. Therefore the 2077 cm^{-1} band observed in Figure 5A does not correspond to a $^{13}C^{18}O$-containing species that has been converted to a

Table 1. Spectroscopic Assignment of Rhodium *gem*-Dicarbonyl Species

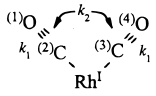

Species	ν_{sym}	ν_{asym}	k_1	k_2	Ref.
	cm^{-1}		(dyne cm^{-1}) × 10^{-6}		
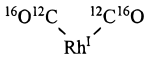	2099	2028	1.721	0.059	[1-6,27-38]
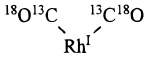	2003	1936	1.726	0.059	This work, [1]
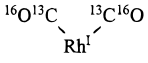	2048	1981			This work, [41]
	(incomplete substitution)				
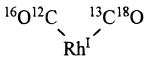	2077	1958			This work
	(2074)	(1955)	(calculated)		
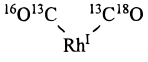	2036	1955			This work
	(2034)	(1949)	(calculated)		
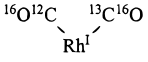	(unobservable)				
	(2082)	(1998)	(calculated)		This work, [41]

$^{13}C^{16}O$-containing species by photoreaction with $^{16}O_2$. Instead it corresponds to the symmetric stretch of the $^{12}C^{16}O$-containing species originating from the photoreaction of $Rh^I(^{13}C^{18}O)_2$ with CO_2 (see Table 1). The 1958 cm^{-1} band corresponds to the antisymmetric stretching mode of the same $Rh^I(^{12}C^{16}O)(^{13}C^{18}O)$ species (see Table 1). On the basis of this experimental comparison of the photochemical reaction of $Rh^I(^{13}C^{18}O)_2$ with either CO_2 or O_2, we assign the 2036 cm^{-1} band produced under CO_2 to the species $Rh^I(^{13}C^{16}O)(^{13}C^{18}O)$ that originates from a CO exchange process in which the dominant gas-phase isotopomer, $^{13}C^{18}O$, has exchanged with $Rh^I(^{13}C^{16}O)(^{12}C^{16}O)$. These processes are summarized in Figure 6. The new infrared bands at 2055 and 2022 cm^{-1} are tentatively assigned to oxidized Rh−$(^{13}C^{18}O)$ species and will be the subject of a subsequent publication.[43]

4. Discussion

1. Photochemistry of $Rh^I(^{13}C^{18}O)_2/Al_2O_3$ in Carbon Dioxide. The production of coordinatively unsaturated $Rh^I(CO)$ sites occurs as a result of the loss of a CO ligand during the ultraviolet photolysis of $Rh^I(CO)_2/Al_2O_3$. Here we have utilized this process to photochemically activate the C−O bond of CO_2 on $Rh^I(CO)$ catalyst sites.

During the ultraviolet photolysis of nonlabeled $Rh^I(CO)_2/Al_2O_3$ in the presence of CO_2 (not presented), essentially no frequency changes were detected in the gem-dicarbonyl infrared bands. To spectroscopically observe the activation of CO_2 on $Rh^I(CO)_2$, isotopically labeled $Rh^I(^{13}C^{18}O)_2/Al_2O_3$ was employed (Figure 1). Irradiation of $Rh^I(^{13}C^{18}O)_2/Al_2O_3$ in CO_2 resulted in the formation of new carbonyl bands at 2077, 2036, and 1958 cm^{-1} indicative of new isotopomers of $Rh^I(CO)_2$ containing ($^{12}C^{16}O$), ($^{13}C^{16}O$), and ($^{13}C^{18}O$) ligands created during CO_2 activation.

2. Identification of the Rh−CO Species Produced during CO_2 Activation. The dissociation of CO_2 on $Rh^I(^{13}C^{18}O)_2/Al_2O_3$ resulted in the formation of the following mixed isotopic gem-dicarbonyl species each exhibiting two spectral lines as shown:

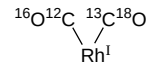

2077 cm^{-1}; 1958 cm^{-1}

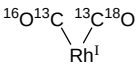

2036 cm^{-1}; 1955 cm^{-1}

1

The assignments are based on the frequencies of the infrared bands developing during photolysis, and the correlation with bands developing during the thermal isotopic exchange experiment (Figures 3 and 4). The infrared bands at 2036 and 1955 cm^{-1} measured during thermal exchange with $^{13}C^{16}O$ agree closely in frequency with the bands at 2036 and 1958 cm^{-1} measured during CO_2 activation, indicating the formation of $Rh^I(^{13}C^{16}O)(^{13}C^{18}O)$ in both cases. The infrared band at 2077 cm^{-1} corresponds to a $^{12}C^{16}O$-containing species. The frequency is too low to be assigned to the symmetric stretching mode associated with unlabeled $Rh^I(CO)_2/Al_2O_3$, occurring at 2099 cm^{-1}.[32−38] It will be assigned to the high-frequency mode of $Rh^I(^{12}C^{16}O)(^{13}C^{18}O)$, with the low-frequency mode occurring near 1958 cm^{-1}.

Unfortunately, two expected bands are not distinguishable in the 1955−1958 cm^{-1} region for the two rhodium gem-dicarbonyl isotopomer species shown in structures **1** above. This is due to the strong negative intensity losses of the overlapping infrared band of $Rh^I(^{13}C^{18}O)_2$ and to the close proximity of the two expected bands. By careful examination of the difference spectra displayed in Figure 4B, one can see the slight shift of the 1958 cm^{-1} feature to lower frequency as more $Rh^I(^{13}C^{16}O)(^{13}C^{18}O)$ species are produced by longer photochemical activation periods.

The C_{2v} structure of $Rh^I(CO)_2$ species on the Al_2O_3 support is well established.[32−38] The surface $Rh^I(CO)_2$ species exist at the coverages investigated here as isolated, noninteracting species since no shift in wavenumber is observed as spectral features intensify during increasing adsorption of CO.[36] Following the method by Knözinger et al.,[41] the frequencies of the high- and low-frequency components of the various isotopic $Rh^I(CO)_2$ (C_{2v}) may be predicted by solving the following secular equation

$$\begin{vmatrix} k_1(\mu_1+\mu_2)-4\pi^2\nu^2 & k_2(\mu_1+\mu_2) \\ k_2(\mu_3+\mu_4) & k_1(\mu_3+\mu_4)-4\pi^2\nu^2 \end{vmatrix} = 0 \quad (1)$$

where μ_i is the reciprocal mass of the ith atom (1 = O; 2 = C; 3 = C; 4 = O); $\mu_i = 1/m_i$, where m_i is the mass of the ith atom; k_1 = force constant for the C−O stretch; and k_2 = force constant for the CO−CO coupling. By using the observed symmetric and antisymmetric stretching frequencies for $Rh^I(CO)_2$, the values of k_1 and k_2 were determined. The same was done for $Rh^I(^{13}C^{18}O)_2$, and the agreement is excellent for the independent measurements, as shown in Table 1. With use of the average k_1 and k_2 values calculated above, ν_{sym} and ν_{asym} of the mixed isotope rhodium gem-dicarbonyl species were determined and

(43) Paper submitted to *J. Am. Chem. Soc.*

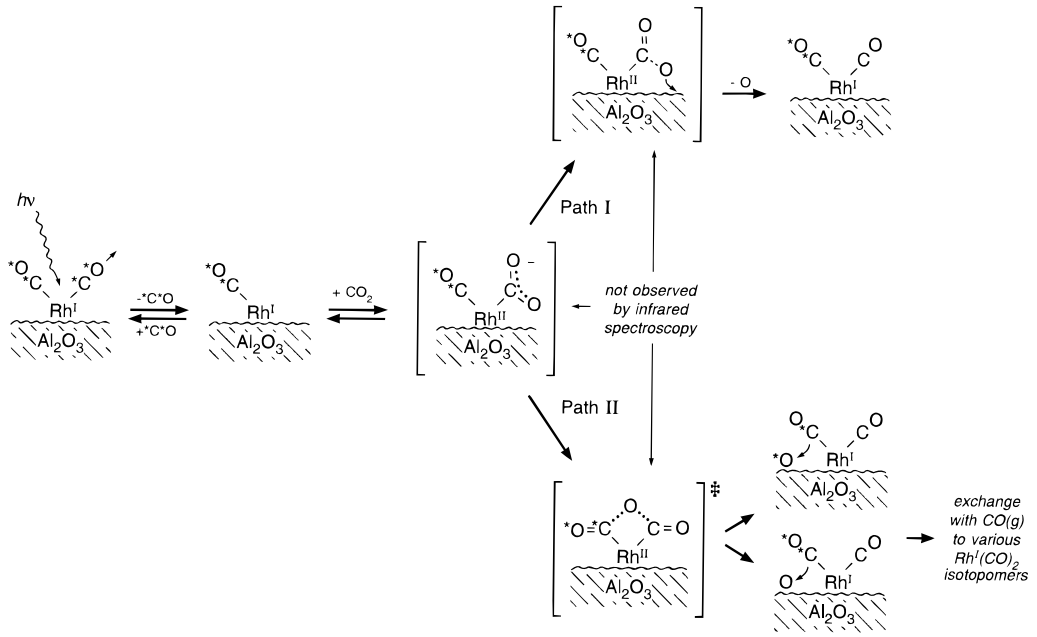

Figure 6. Proposed mechanism for the activation of CO_2 on photochemically generated $Rh^I(^{13}C^{18}O)$ sites.

are listed in Table 1 along with the experimentally measured frequencies. Discrepancies between calculated and measured frequencies [-3 cm^{-1} and -3 cm^{-1} for $Rh^I(^{12}C^{16}O)(^{13}C^{18}O)$; -2 cm^{-1} and -6 cm^{-1} for $Rh^I(^{13}C^{16}O)(^{13}C^{18}O)$] are within expectations considering the experimental difficulties encountered when determining precise frequencies for the overlapping bands.

3. The Formation of a $Rh^I(CO)(CO_2)$ Complex. The activation of CO_2 requires the coordination of CO_2 onto a Rh center. Several transition metal complexes have been prepared that utilize CO_2 as ligands.[9-11] The type of coordination depends on the metal, ligands, and surrounding conditions. On a single metal site, three basic types of bonding may occur between the metal and CO_2, labeled here as Type I, Type II, and Type III, as shown below:

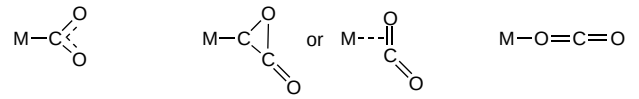

η^1-complex Type I | η^2- or π-complex Type II | end-on complex Type III

Type I complexes represent η^1 bonding between the metal center and CO_2. Electron density is donated by the metal center to the carbon atom of CO_2. Complexes of Type II involve η^2 bonding, or side-on bonding, between the metal center and the carbon atom and an oxygen atom of CO_2. It is often not possible to distinguish three-membered ring bonding from π-complexing since the structures are spatially similar. Type III (end-on) complexes involve coordination of CO_2 only through lone pairs of an oxygen atom, and this is considered to be the least probable type of complexing.[9-11] For Types I and II complexes, a bent geometry is adopted for the CO_2. The linear geometry for CO_2 is retained in Type III complexes.

The type of CO_2 complex may be deduced from the infrared spectra. In general, two infrared stretching bands are observed for the antisymmetric and symmetric stretching modes of metal-coordinated CO_2. The antisymmetric stretching mode, ν_{asym}, falls into the range 1800$-$1500 cm^{-1} and the symmetric mode, ν_{sym}, occurs in the range 1600$-$1100 cm^{-1}.[9] The infrared bands for $Rh(diars)_2(Cl)(CO_2)$ [diars = *o*-phenylene-bis(dimethylarsine)] Type I complex with η^1 bonding were reported at 1610 and 1210 cm^{-1}.[14] Rh$-$(CO_2) complexes with η^2 bonding (side-on) exhibit infrared bands in the ranges 1798$-$1630 and 1592$-$1120 cm^{-1} for each mode.[15,16] There are no examples of Rh complexes that exhibit Type III (end-on) bonding with a CO_2 ligand.

During the activation of CO_2 on $Rh^I(^{13}C^{18}O)_2/Al_2O_3$, infrared features are observed between 1800 and 1200 cm^{-1} (Figure 2). These modes have been assigned to bicarbonate and carbonate species produced when CO_2 adsorbs onto the Al_2O_3 support. Although the frequencies of these spectral bands correspond to the frequency ranges listed for CO_2 coordinated on Rh, no new features or outstanding differences in line shape are observed when comparing the photoactivation of CO_2 to the adsorption of CO_2 in the absence of ultraviolet light (Figure 2). Only a slight increase in the amount of bicarbonate/carbonate produced is detected during the photoactivation of CO_2. Since spectral features corresponding to any known mode of CO_2 bonding to Rh centers are not observed, we conclude that these intermediate species are of low surface concentration and/or that they exhibit low extinction coefficients compared to the carbonyl ligands in $Rh^I(CO)_2$.

The assignments of the bicarbonate/carbonate modes and the frequency ranges for transition metal$-$$CO_2$ complexes are summarized in Table 2.

4. Mechanism for CO_2 Activation. Due to its isolated nature and to its ionic character, the chemistry of rhodium gem-dicarbonyl species better resembles the chemistry of organometallic complexes than the chemistry of CO chemisorbed on metallic surfaces. The proposed mechanism for CO_2 activation on $Rh^I(^{13}C^{18}O)_2/Al_2O_3$ is shown in Figure 6 (the isotopic labels are indicated by an asterisk). The photolysis of $Rh^I(^{13}C^{18}O)_2$ species results in the reversible loss of a carbon monoxide ligand to form coordinatively unsaturated $Rh^I(^{13}C^{18}O)$ sites. These sites may either adsorb a $^{13}C^{18}O$ molecule from the gas phase to regenerate gem-dicarbonyls or coordinate with CO_2. The formation of an intermediate Type I complex with η^1 coordination between the Rh center and the carbon atom of CO_2 is postulated. If the coordination occurred though η^2 bonding, as in the Type II complex, one would expect to see the formation of oxidized Rh^{II} or Rh^{III} carbonyl species following CO_2

Table 2. Spectroscopic Assignment of Bicarbonate/Carbonate Modes and Transition Metal Carbon Dioxide Modes

species	cm^{-1}	cm^{-1}	cm^{-1}	ref
HCO_3^-	1648−1637	1470−1490	1230−1238	39,40,42
CO_3^{2-}		1450		39,42
HCO_3^-/CO_3^{2-}	1646	1445	1228	This work

species	bonding	ν_{asym}, cm^{-1}	ν_{sym}, cm^{-1}	ref
transition metal carbonyl complexes of CO_2		1800−1500	1600−1100	9
$Rh(diars)_2(Cl)(CO_2)$[a]	η^1	1610	1210	14
$Rh[P(n\text{-}Bu)_3]_2(Cl)(CO_2)$ (isomers)	η^2	1668,1630	1165,1120	16
$Rh[HC(CH_2CH_2P(t\text{-}Bu)_2)_2](CO_2)$	η^2	1798	1592	15

[a] [diars = *o*-phenylene-bis(dimethylarsine)].

activation, as shown below:

No stable oxidized rhodium carbonyl species were produced during CO_2 activation, as indicated by the observation that there was no correlation between the infrared features observed during CO_2 activation and the features detected when $Rh^I(^{13}C^{18}O)_2/Al_2O_3$ was irradiated with ultraviolet light in the presence of oxygen (Figure 5). The lack of formation of oxidized rhodium carbonyl species suggests that η^2 bonding does not occur during CO_2 coordination on Rh sites.

The η^1 bonding is favored by electron rich transition metals that can donate electron density into the π^* orbital of CO_2 thereby reducing the C═O bond strength.[9−11] Reversible η^1 coordination of CO_2 with a d^8 Rh^I center leads to a high partial negative charge on the CO_2 fragment. The electron transfer causes CO_2 instability, and the CO_2 anionic fragment adopts a more energetically favorable bent geometry.[7,9] Dissociation of CO_2 may then occur. In our case, the dissociation of CO_2 occurs by two postulated pathways. As shown in the reaction scheme of Figure 6, Path I involves the dissociation of a C−O bond in the CO_2 ligand and the liberation of an oxygen atom. The fate of the O atom cannot be determined in this work. Mixed isotopic rhodium gem-dicarbonyl species of the form $Rh^I(^{12}C^{16}O)(^{13}C^{18}O)$ are generated in the process. Path I represents the dominant activation channel.

Path II is responsible for the $Rh^I(^{12}C^{16}O)(^{13}C^{18}O)$ and $Rh^I(^{12}C^{16}O)(^{13}C^{16}O)$ isotopic species. The production of a $^{13}C^{16}O$-containing surface species is evidence for oxygen atom exchange occurring rapidly between the CO_2 fragment and the other CO ligand followed by either ^{18}O or ^{16}O loss. A similar oxygen transfer process was observed by Cooper and co-workers[44] with $Fe(\eta\text{-}C_5H_5)(CO)_2(CO_2)^-$ complexes. Unfortunately we are not able to distinguish clearly between the two isotopic species produced in Path II. Both $^{12}C^{16}O$-containing species yield unresolved symmetric stretching modes in the range 2082−2077 cm^{-1}. For $Rh^I(^{12}C^{16}O)(^{13}C^{16}O)$, the antisymmetric mode is expected to be at 1998 cm^{-1}, and this is strongly overlapped by the intense 2003 cm^{-1} mode of the original $Rh^I(^{13}C^{18}O)_2$ species. In addition, continuous exchange of surface dicarbonyls with the various isotopomers of gas-phase CO occurs as photolysis proceeds, and all mixed isotopic dicarbonyls are eventually produced.

The oxygen atoms generated during the dissociation presumably transfer to the aluminum oxide support. These oxygen atoms may assist in the formation of bicarbonate/carbonate species. Slightly more intensity was observed for the infrared bands for bicarbonate/carbonate during the photoactivation of CO_2 than for the thermal adsorption of CO_2 (Figure 2); however, there was no obvious evidence for the presence of isotopically labeled species. Raskó and Solymosi[45] reported that the photoinduced dissociation of CO_2 on Rh/TiO_2 surfaces is mediated by filling surface vacancy sites with oxygen atoms from CO_2. A similar process may exist here with oxygen atoms filling vacant anion sites in the Al_2O_3 surface.

5. Conclusions

The following conclusions have been reached concerning the activation of CO_2 on coordinatively unsaturated $Rh^I(CO)$ sites produced photochemically from $Rh^I(CO)_2$.

(1) Carbon dioxide is activated on photochemically produced $Rh^I(^{13}C^{18}O)$ sites to produce isotopically labeled rhodium gem-dicarbonyls. The two major products show infrared bands at 2077 and 1958 cm^{-1} assigned to the formation of $Rh^I(^{12}C^{16}O)(^{13}C^{18}O)$ species and bands at 2036 cm^{-1} and near 1958 cm^{-1} assigned to the formation of $Rh^I(^{13}C^{16}O)(^{13}C^{18}O)$.

(2) The formation of two unique isotopomers of the rhodium gem-dicarbonyl species containing $^{12}C^{16}O$ and $^{13}C^{16}O$ is indicative of two distinct pathways for CO_2 activation, as shown in Figure 6. Path I involves direct dissociation of the C−O bond in bound CO_2 ligands and Path II involves oxygen atom exchange between CO_2 and CO ligands followed by C−O bond dissociation in the exchanged CO_2 ligand.

(3) The surface intermediate involving CO_2 is postulated to have η^1 bonding between the Rh center and CO_2. Side-on or η^2-type bonding is not observed since no oxidized rhodium carbonyl species are observed during CO_2 activation.

(4) This work demonstrates the first steps of a potential low-temperature route for the conversion of CO_2 into other molecules on catalyst sites through CO formation with ultraviolet light as an energy source.

Acknowledgment. We thank the Department of Energy, Office of Basic Energy Sciences for support of this work.

JA9804114

(44) Lee, G. R.; Cooper, N. J. *Organometallics* **1985**, *4*, 794.

(45) Raskó, J.; Solymosi, F. *J. Phys. Chem.* **1994**, *98*, 7147.